Drying kinetics and heat flux in thin-layer conductive drying

Olivier Fudym, Christine Carrere Gee, Didier Lecomte, Bruno Ladevie

DRYING KINETICS AND HEAT FLUX IN THIN-LAYER CONDUCTIVE DRYING

O. Fudym, C. Carrère-Gée, D. Lecomte, B. Ladevie
Ecole des Mines d'Albi, Centre Energétique - Environnement
UMR CNRS 2392 Laboratoire de Génie des Procédés des Solides Divisés
Route de Teillet, 81013 Albi - France

(Communicated by M. Lebouche and J. Taine)

ABSTRACT

Thin-layer drying by coating of a viscous product on a hot metallic surface is studied from the point of view of heat and mass transfer. An experimental device has been built up in order both to provide and to estimate the heat flux density at the interface between the hot plate and the drying sample. Results are presented for alumina sludge drying. The determination of the interfacial heat flux is obtained from temperature measurements in the metallic plate and the solution of an inverse conduction problem. An analytical direct model is made using the quadrupole formalism and the system transfer function is calculated. The inverse problem is solved using Beck's sequential function specification method. Intrinsic drying kinetics are obtained by an energy balance.

Introduction

Among contact drying technologies, drum drying is widely used to treat heat-sensitive products in the food industry. The product is sprinkled or coated on a hot rotating cylinder. The wall temperature is above boiling temperature and the thin-film of product dries by vaporization. Absence of mixture and agitation constitutes an advantage for viscous products like sludge or pastes, enabling a good control of the residence time, and average water content. However, drying rates, when involved in a vaporization thin film process, are very difficult to measure:

- Thin-film boiling is very fast, making product sampling impossible.
- Mass losses occur in a very short time, with high heat transfer rates. It is thus necessary both to provide intense heat transfer ($1\,MW/m^{-2}$) with an adequate heating system and to measure small mass variations ($\leq 3\,g$) in a short time ($1-5\,s$).

It would have been possible to generate a large heat flux density with an electric heater or with a condensable fluid but we would have encountered significant technological problems like temperature control and thermal inertia effects. Furthermore, the accuracy of commercial scales decreases with the maximum load and in the present case would have been of the same order of magnitude as the mass loss

($\cong 1\,g$), which was not acceptable. The supply and measurement of intense flux during the process was a technical challenge and the solution of a thermal condensator (large thermal capacity and large thermal diffusion properties) was adopted. An indirect method was chosen to estimate drying rates and measure the interfacial heat flux instead of the mass loss.

Experimental Device and Instrumentation

The first objective of this experimental device was to produce thermal conditions for thin-film vaporization contact drying. It was shown by Vasseur [1] that very high heat flux densities ($\approx 10^5$-10^6 $W.m^{-2}$) are exchanged during the first instants for viscous foodstuff thin-film drying, due to the low product thickness. It was important, in the experimental device to be designed:

- to keep wall temperature at a value higher than 100°C in spite of a very high flux density.
- to be able to measure the interfacial temperature and the interfacial heat flux density with limited experimental errors (non-intrusive measurements).

The principle of the designed experimental device is simple: a metal plate acting as a thermal condensator was placed in a convective loop [2] and brought to an initial temperature above the theoretical boiling temperature of water. The plate was thick enough in order to store the energy amount necessary for complete drying and diffusive enough to ensure high heat flux densities at the interface. Copper was chosen for its excellent heat transfer and energy storage properties. During coating, water is vaporized and the product's thin-layer (0.7 mm thickness) dries in a very short time.

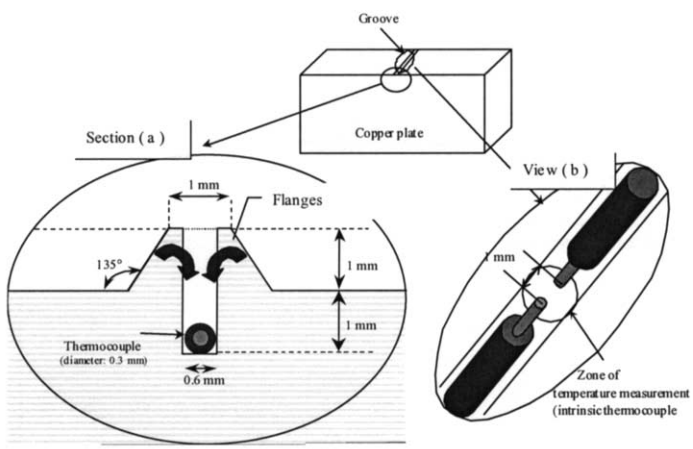

FIG. 1
Different views of the wires of the thermocouples on the top side of the copper plate before hammering the flanges into the groove. Cross section (a) shows the position of the thermocouple in the groove. View (b) shows that the thermocouple will be formed after hammering by the contact between the wires and the copper. The contact zone is a cylinder of 0.3 mm diameter and 1mm length.

The second goal was to estimate the interfacial heat flux between the drying product and the heated plate. The surface temperature could not be measured directely: a sensor located on the top side would disturb the material coating, as well as heat transfer. Two thin thermocouple wires (0.3 mm) were laid inside a groove cut over the width of the plate (FIG. 1). A macrophotography of the plate cross section confirms that the vicinity of the sensor was very homogeneous due to the ductility of copper and that very good contact between wire and copper was achieved. The resulting thermocouple, with separated contacts, is laid in a direction parallel to isothermal planes. Before carrying out this delicate operation on the plate, several reproducibility tests were carried out in order to check the exact location of measurement (0.85 mm depth from front side). The local temperature is derived from the average value of the Seebeck e.m.f. in the volume bounded by the two stripped ends of the wires (FIG.1, *view b*) . It has been shown from sensitivity analysis that the error on the location of the thermocouple had little influence on heat flux calculations.

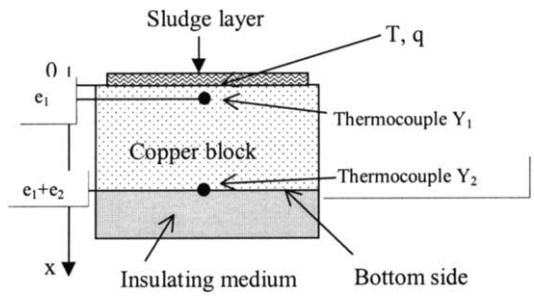

FIG. 2
Schematic experimental device

An other sensor was laid out on the plate's bottom side (Y_2 on FIG. 2). The large interfacial heat flux imply large thermal gradients close to the top side, thus the measured temperature Y_1 is different from the actual wall temperature. Thus, the wall temperature T and heat flux density q are estimated from inside temperature measurements and an inverse heat conduction method is achieved.

Direct Model

A direct one dimensional model was built in order to simulate the sensor temperature evolution (FIG. 2). The quadrupole method [3] is used to calculate the formal relationship between the interfacial heat flux q and the theoretical temperature T_1 at the location of thermocouple 1.The sample is assumed homogeneous and, initially, the whole system is assumed to be at a uniform temperature T_0. The corresponding equation is

$$\frac{\partial^2 T}{\partial x^2} = \frac{1}{a}\frac{\partial T}{\partial t} \tag{1}$$

with a known heat flux density at the plate surface $x = 0$ and an insulated bottom at $x = e$. A Laplace transform is applied to Eq. (1) such as $\theta(x,s) = \int_0^\infty (T(x,t) - T_0)e^{-st}dt$:

$$\frac{d^2\theta}{dx^2} = \frac{s}{a}\theta \tag{2}$$

The Laplace transformed heat flux is:

$$\phi(x,s) = -\lambda\frac{d\theta(x,s)}{dx} \tag{3}$$

Expressions (2) and (3) are then arranged in the thermal quadrupole form [4]:

$$\begin{bmatrix}\theta\\ \phi\end{bmatrix} = \begin{bmatrix}A_1 & B_1\\ C_1 & D_1\end{bmatrix}\begin{bmatrix}\theta_1\\ \phi_1\end{bmatrix} \tag{4}$$

$$\begin{bmatrix}\theta_1\\ \phi_1\end{bmatrix} = \begin{bmatrix}A_2 & B_2\\ C_2 & D_2\end{bmatrix}\begin{bmatrix}\theta_2\\ 0\end{bmatrix} \tag{5}$$

where $A_i = D_i = ch(k.e_i)$ (6)

$$B_i = \frac{sh(k.e_i)}{k\lambda} \tag{7}$$

$$C_i = k\lambda sh(k.e_i) \tag{8}$$

and $$k = \sqrt{\frac{s}{a}} \tag{9}$$

It is then possible to determine the transfer functions $F_i(s)$) between the Laplace transformed superficial heat flux, and temperatures θ_i such as

$$\theta_i = F_i(s).\phi, \quad i = 1,2 \tag{10}$$

An inverse method allows calculating the superficial heat flux density $q(t)$ from the measured temperatures $Y_1(t)$, and the corresponding temperature $T_1(t)$ from the direct model. Inverse transfer functions $f_i(t)$ are obtained from a numerical Laplace inversion of $F_i(s)$ [5]. Temperature $T_i(t)$ is then computed by a convolution product:

$$T_i(t) - T_0 = \int_0^t q(t-\tau).f_i(\tau)d\tau \tag{11}$$

The transfer function between $q(t)$ and the computed temperature $T_1(t) - T_0$ at sensor location 1 is

$$F_1(s) = \frac{A_2}{C_1A_2 + D_1C_2} \tag{12}$$

The insulated boundary condition will be validated by comparison of $T_2(t)$ with the measured temperature $Y_2(t)$ of the bottom side of the copper block..

Inverse Method

In the case of one-dimensional linear problem with fast and high heat flux variations, a sequential method is adapted. The function specification method with a sequential constant heat flux functional form is used [6]. For this method, $q(t)$ is approximated in a discrete form:

$$q = [q_1 \quad q_2 \quad ..... \quad q_i \quad q_{i+1} \quad ..... \quad q_n] \tag{13}$$

where $q_i = q(t_i) = q(i\,dt)$. Eq. (11) can be expressed in a discrete form:

$$T_i - T_0 = T_1(t_i) - T_0 = \sum_{j=1}^{i} f_1(t_i - t_j).q_j.dt = dt.[q_1 f_i + q_2 f_{i-1} + ... + q_{i-1} f_2 + q_i f_1] \tag{14}$$

where $f_j = f_1(t_j)$ and $T_i = T_1(t_i)$. Assuming that $q_1,...,q_i$ and $T_1,...,T_i$ are known, q_{i+1} is searched by an ordinary least square procedure using the next $Y_{i+1},...,Y_{i+r}$ measurements, assuming a constant heat flux q_{i+1} during the *r* future time steps (FIG. 3):

$$q_{i+1} = q_{i+2} = ... = q_{r-1} = q_r \tag{15}$$

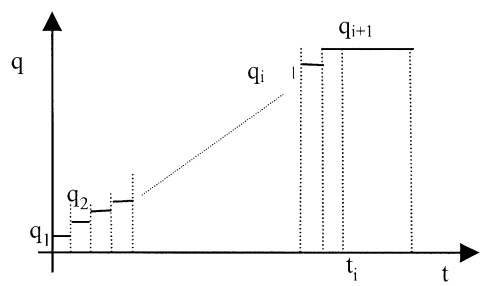

FIG. 3
Time discretization at time step t_i

The least square procedure minimizes the functional form J with respect to q_{i+1}:

$$J(q_{i+1}) = \sum_{j=1}^{r} \left(Y_{i+j} - T_{i+j}(q_{i+1})\right)^2 \tag{16}$$

Equation (16) is differentiated with respect to q_{i+1} and set equal to zero:

$$\frac{\partial J(q_{i+1})}{\partial q_{i+1}} = -2\sum_{j=1}^{r} \left(Y_{i+j} - T_{i+j}(q_{i+1})\right)\frac{\partial T_{i+j}}{\partial q_{i+1}} = 0 \tag{17}$$

The heat flux increment δq during the time step is searched:

$$q_{i+1} = q_i + \delta q \tag{18}$$

According to Eq. (15), the r future computed temperatures $T_{i+j}(q_{i+1})$ can be written:

$$T_{i+j}(q_{i+1}) = T_{i+j}(q_i) + \frac{\partial T_{i+j}}{\partial q_i}\delta q \tag{19}$$

The sensitivity coefficients in Eq. (17) and Eq. (19) are equal:

$$S_j = \frac{\partial T_{i+j}}{\partial q_{i+1}} = dt\sum_{k=1}^{j} f_k \tag{20}$$

$$S_j \approx \frac{\partial T_{i+j}}{\partial q_i} = dt\ f_{j+1} \tag{21}$$

and: $$\sum_{j=1}^{r}\left(Y_{i+j} - T_{i+j}(q_i) - dt\ f_{j+1}\ \delta q\right)S_j = 0 \tag{22}$$

Eqs. (17 – 22) yields the heat flux increment δq for q temporarily assumed constant. This equation is used in a sequential way by incrementing i by one at every time step.

$$\delta q = \frac{\sum_{j=1}^{r}\left(Y_{i+j} - T_{i+j}(q_i)\right)S_j}{dt\sum_{j=1}^{r} S_j\ f_{j+1}} \tag{23}$$

If r is small, then $S_j \approx f_{j+1}$ and:

$$\delta q = \frac{\sum_{j=1}^{r}\left(Y_{i+j} - T_{i+j}(q_i)\right)\sum_{k=1}^{j} f_k}{dt\sum_{j=1}^{r}\left(\sum_{k=1}^{j} f_k\right)f_{j+1}} \tag{24}$$

The sensitivity coefficients in Eq. (24) are known from Eq. (14) with i replaced by $i+1$ to $i+r$. For example, the temperature T_{i+j} at time t_{i+j}, with the assumption of constant heat flux after time t_i, can be expressed as:

$$T_{i+j} - T_0 = dt.\left[q_1 f_{i+j} + q_2 f_{i+j-1} + \ldots + q_{i+j-1} f_2 + q_{i+j} f_1\right] \tag{25}$$

Assuming Eq. (14) yields the sensitivity coefficients, with $j = 1$ to r:

$$S_{i+j} = S_j = S(j) = dt.\left[f_1 + f_2 + \ldots\ldots\ldots\ldots + f_{j-1} + f_j\right] \tag{26}$$

Having a direct model with a convolution such as Eq. (11) coupled with the specification function method is of great interest: the sensitivity coefficients are constant with time step, and only the first $r+1$ values of the inverse transfer function are to be calculated. The sum of inverse transfer function values in

Eq. (26), since $f(t)$ is positive, also implies S_{i+j} increases with j. This property improves the future time steps stabilization effect in Eq. (24), because each future time step number increment will contribute with a growing sensitivity coefficient. Sensitivity analysis is to be detailed in the next section.

Sensitivity Analysis

The reduced sensitivity coefficient of T_1 to a parameter β_j is computed by finite difference as:

$$S_j(t) = \beta_j \frac{T_1(t, \beta_j + \delta\beta_j) - T_1(t, \beta_j - \delta\beta_j)}{2\delta\beta_j} \tag{27}$$

Reduced sensitivity coefficients to the main parameters are plotted on FIG. 4. It is shown that the sensitivity of T_1 to e_1 is very small. This is due to the sensor location near the surface. Sensitivity coefficients to thermal conductivity λ and thermal diffusivity a have the same order of magnitude as the sensitivity coefficients to the plate thickness e_2. The values of these sensitivity coefficients are high. It is thus important to have a good knowledge of the plate thermal properties. These properties were measured with 5% accuracy at 400K. The sensitivity to the mean heat flux φ_0 is very high at the beginning of the drying process. The determination of this mean heat flux density is delicate. It is necessary to have a sufficiently small time step to make sure that the estimated value is correct and a very low noise on the measurement of temperature Y_1 is required.

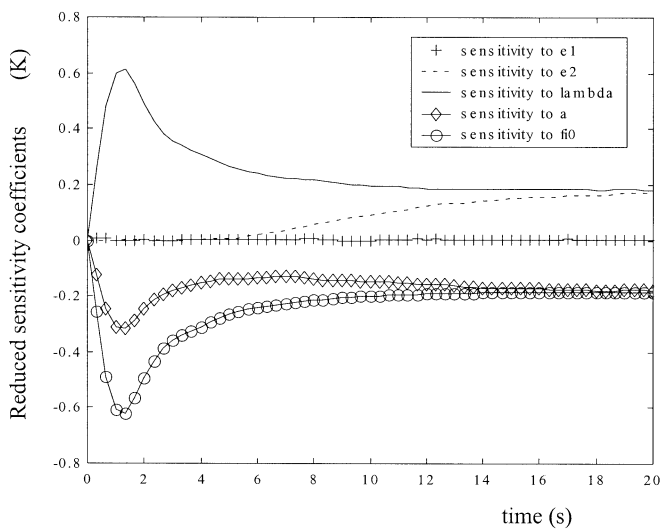

FIG. 4
Reduced sensitivity coefficients

Equation (14) can be written in a matrix form, in order to express the sensitivity matrix $\mathbf{X}$ to the unknown heat flux components:

$$\mathbf{T} = \mathbf{X}\mathbf{q} \tag{28}$$

where $\mathbf{X} = dt.\begin{bmatrix} f_1 & 0 & 0 & \dots & \dots & \dots & 0 \\ f_2 & f_1 & 0 & \dots & \dots & \dots & 0 \\ f_3 & f_2 & f_1 & 0 & \dots & \dots & 0 \\ . & f_3 & f_2 & f_1 & \dots & \dots & . \\ . & \dots & \dots & \dots & .. & \dots & . \\ . & & & . & . & f_1 & 0 \\ f_n & \dots & \dots & \dots & f_3 & f_2 & f_1 \end{bmatrix}$

Due to the steep exponential decrease of the transfer function $f(t)$, the sensitivity coefficients, obtained from Eq. (28) and the X matrix coefficients, are non zero only for a few points very close to each heat flux component q_i at time t_i. Thus, a whole time domain estimation procedure would be difficult to regularize: the q_i component at time t_i can only be estimated very close to the corresponding time t_i. The sensitivity coefficients for the sequential method $S(r)$, defined by Eq. (26), are plotted on FIG. 5 as a function of the number of future times steps r. This curve makes clear the interest of the present algorithm, and the future time steps stabilization effect, since the sensitivity coefficients increase with the number of future time steps.

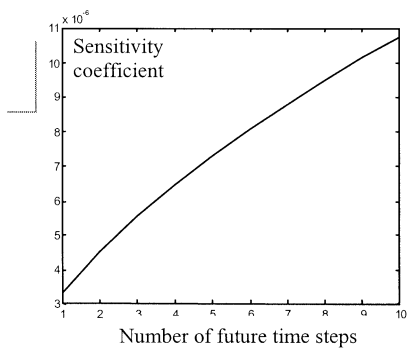

FIG. 5
Sensitivity coefficients $S(r)$ as a function of the future time steps number r

Heat Flux Estimation Results

Before to be applied to the real experiments shown in this section, numerical experiments have been simulated in order to validate the method, in conditions close to the experimental problem, and have proved its efficiency. These numerical validation tests are not presented here.

The plate is placed inside a drying loop, and a stable initial temperature above the product's boiling temperature is reached before the experiment is started. At time $t = 0$, the product is quickly coated on the plate, while Y_1 and Y_2 acquisition starts. Although a large number of experiments has been made [7], the results are presented here only for two cases, with initial temperature $T_0 = 138°C$ and $T_0 = 114°C$. The chosen time step is dt = 0.01 s, the number of estimated parameters is n = 2518, and the number of future time steps r is 5. The discrete Fourier number $\frac{a\,dt}{e_1^2}$ is 1.30 10^{-3}. Measured and computed temperatures history are ploted on FIG. 6. The measured sensor temperature Y_1 is perfectly fitted with T_1, but this result is the consequence of the inverse method, very close to an exact matching algorithm. More important is the perfect fit between the bottom side measured temperature Y_2 and the computed temperature T_2. This result means that a good agreement is obtained between the experimental results and the 1D model, and proves the validity of bottom side insulated boundary condition assumption. Wall temperature T and T_1 are different at the beginning of the experiment due to the large heat flux densities. This difference becomes negligible after *2* seconds.The measured temperature Y_1 decreases strongly in the first seconds following the coating ($\approx 12°C$) due to sudden boiling phenomena, and the corresponding superficial high heat flux density. The decrease is stopped when the heat flux intensity falls down while thermal diffusion inside the copper plate tends to homogenize the temperature. When $q(t)$ is near zero, top and bottom side temperatures tend to the same value, corresponding to a quasi-steady state transfer.

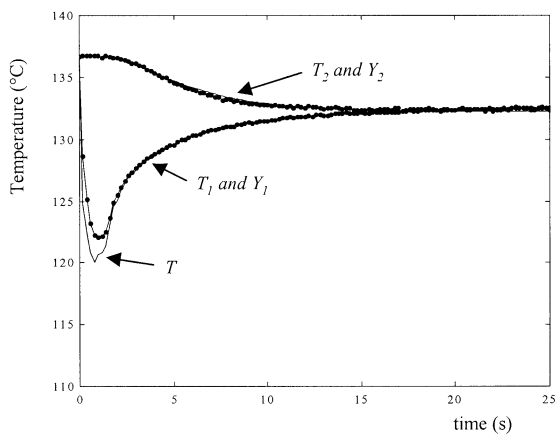

FIG. 6
Computed and measured temperatures at the sensor locations *1* and *2*
for initial temperature $T_0 = 138°C$

The experimental temperature Y_2 decreases slowly due to thermal diffusion through the thickness of the copper block after a first period where Y_2 is assumed constant. At the end of the experiment ($t = t_f$), the two temperatures Y_1 and Y_2 are equal and the copper block temperature is homogeneous. The wall temperature T is always above the product boiling temperature. Boiling transfer stops probably due to a change in the product structure.

FIG. 7 shows the computed and measured temperatures for an initial temperature $T_0 = 114°C$. The driving force for boiling is much smaller but the changes in temperatures Y_1 and Y_2 are very similar to the previous experiment. At the end of this experiment, the computed temperature T_2 differ widely from Y_2. In that case, the hypothesis concerning the insulated bottom wall is no more valid, and it would be necessary to use the Y_2 data as a boundary condition in the model.

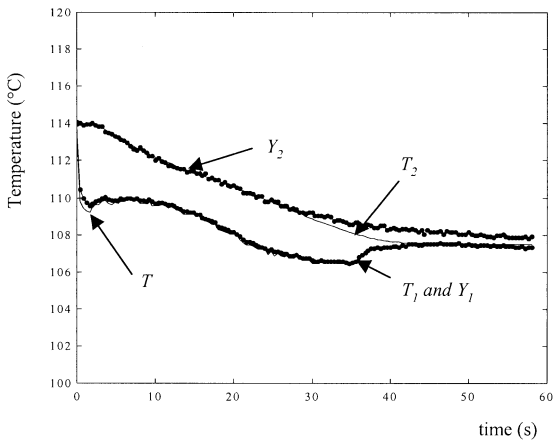

FIG. 7
Computed and measured temperatures at the sensor locations *1* and *2*
for initial temperature $T_0 = 114°C$

FIG. 8 shows the superficial heat flux density $q(t)$ after estimation from Y_1 measurements at $T_0 = 138°C$. A high value of about 10^6 W.m^{-2} is reached after a very short time (less than one second), due to boiling phenomena. This intense heat flux is followed by a second period where boiling is progressively slowing down and followed by an evaporative drying period, involving smaller heat transfer. The transition period between boiling and evaporation drying is not clearly defined, but on the process point of view, the first period is the fastest and the most desirable.

The boiling time is defined by the time gap for which the heat flux density has large values (typically when boiling conditions occur). FIG. 9 shows that the maximum heat flux and the shortest boiling times are obtained with large temperature differences between the copper block and the boiling temperature.

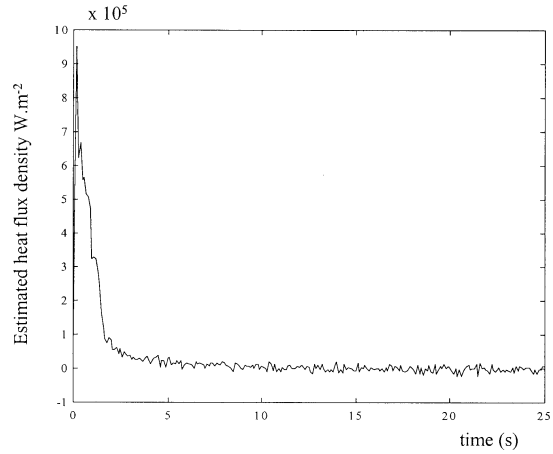

FIG. 8
Estimated superficial heat flux density $q(t)$ for initial temperature $T_0 = 138°C$

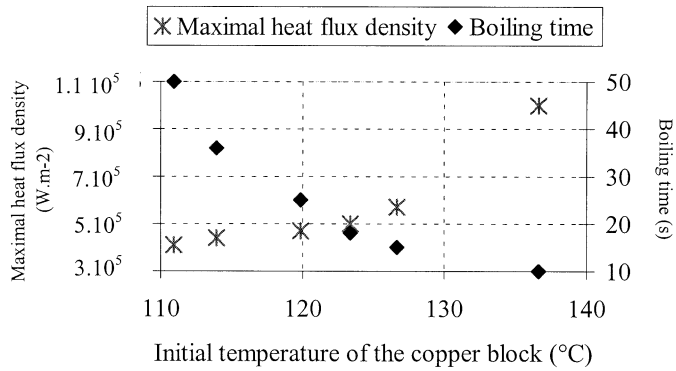

FIG. 9
Influence of the initial temperature on boiling time and heat flux density

Energy Balance and Drying Curves

The superficial heat flux can be used to calculate the amount of energy E transferred from the copper block to the coated material between time $t = 0$ and t:

$$E(t) = \int_0^t q(\tau) d\tau \tag{29}$$

At the end of the process, top side and bottom side temperatures are equal to the final temperature T_f and from a simple energy balance of the copper block, the overall energy lost by the copper plate E' may be calculated :

$$E' = \rho c_p .e.(T_f - T_0) \tag{30}$$

TABLE 1
Comparison of two energies E' and $E(t_f)$ for various initial temperatures of the copper plate

T_o (°C)	$E(t_f)$ (x10^5 J.m^{-2})	E' (x10^5 J.m^{-2})
138	9.10 ± 0.01	8.91 ± 0.89
127	9.08 ± 0.01	9.18 ± 0.92
123	8.88 ± 0.01	8.95 ± 0.90
120	10.07 ± 0.02	10.01 ± 1.01
114	13.39 ± 0.02	13.38 ± 1.34
111	14.83 ± 0.02	14.51 ± 1.45

E' is found to be quite close to $E(t_f)$, where t_f is the final time when $T_1 = T_2 = T_f$, as shown in TABLE 1. This implies that $q(t)$ is the only flux crossing plate walls. This result confirms the insulated back side assumption, but also confirms the "no lateral losses" assumption, hence the one dimensional conductive transfer assumption is valid in the range of the performed experiments. No direct method could be used to determine with precision the dry matter load M during the coating process because of the difficulty to scrap and weigh the fully dried solid. But a simple energy balance of the moisture content during the thin-film drying experiment allows an indirect calculation of M :

$$M = \frac{E'}{(W_0 - W_f)l_v(T_0)} \tag{31}$$

where W_0 and W_f are the initial and final moisture contents of the dried product which can be easily determined experimentally. The moisture content $W(t)$, the drying curves, and finally the drying rate can be deduced from Eqs. (29 - 31):

$$W(t) = W_0 - \frac{E(t)}{M.l_v(T_0)} \tag{32}$$

From the relative error made on the determination of the energy for drying E, the relative errors on the dry matter load and on the water content are determined. For a typical experiment, these values are respectively 2.3% and 3.7%.

Drying curves are shown on FIG. 10. It is noticeable that thin-layer drying, in that particular case, is very fast, thanks to the non-internal transfer limitation. The drying time is increasing with the initial temperature T_0 and the dry matter load M. The final water content, except for the two experiments

where the dry matter load was very low, was close to *1kg/kgDB*. This value of the moisture content corresponds to the transition between free and bound water of the alumina sludge. Heat transfer is limited by conduction effects and the dominant phenomena for drying is a combination of internal moisture migration and evaporation. For smaller dry matter load at $T_0 = 138°C$, the internal effects have less influence and complete drying is possible in a short time, which tends to prove that with a high block temperature and a small load, the material temperature can be kept over the boiling temperature.

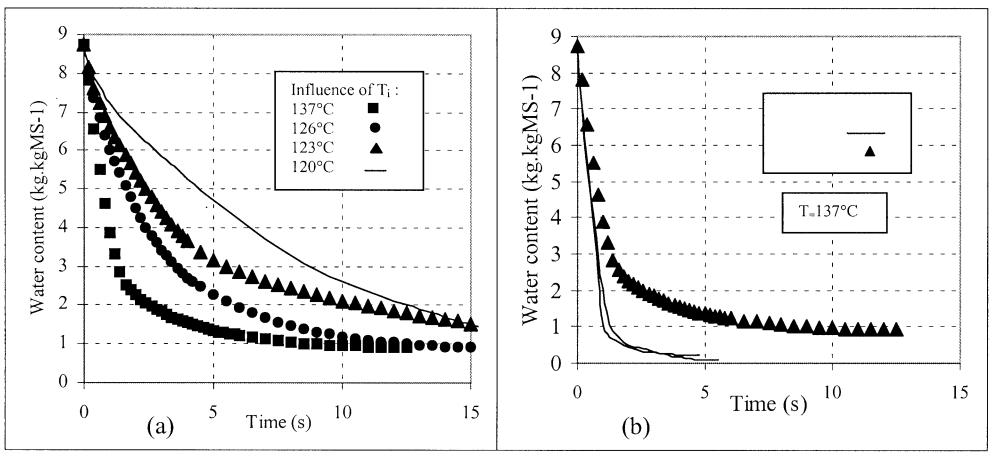

FIG. 10
Drying curves calculated for (a) various initial temperature T_0 (b) different dry matter load M

Determination of a Thermal Resistance

From the interfacial heat flux density and the wall temperature, it is possible to define a thermal resistance between the sludge and the copper plate, assuming the temperature T_b of the thin layer is homogeneous and equal to the boiling temperature (*100°C*) during the process [2] :

$$R_{ext}(t) = \frac{T(t) - T_b}{q(t)} \tag{33}$$

FIG. 11 shows the change of the thermal resistance with the water content for different initial temperatures of the copper plate. The dry matter load has little effect on the evolution of this thermal resistance. Thermal resistance is reduced when initial temperature of copper increases, and is increased when water content reduces due to the setting of a thin insulating layer. Boiling transfer stops probably due to the product structure evolution: a high thermal resistance is found between the dried product and the plate interface. The noisy values of the thermal resistance are due to the important decrease of the heat flux. Obviously, equation. (33) is no more convenient when the transition occurs to evaporation.

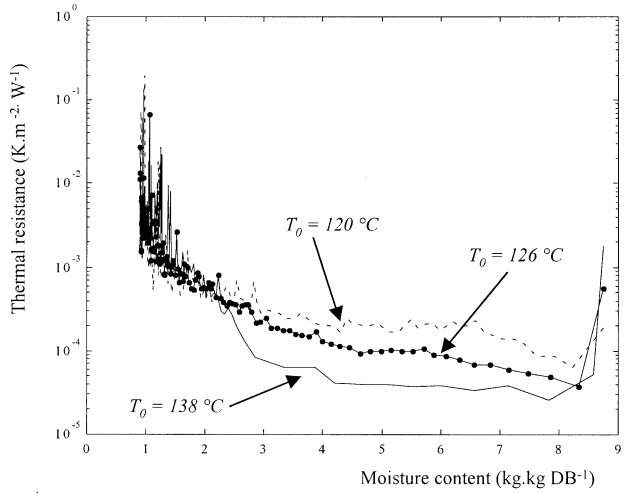

FIG. 11
Thermal resistance change v.s. moisture content for different wall temperatures

Conclusion

The present study has been developed in order to characterize heat and mass transfer rates in thin-layer contact drying and to determine drying curves. To cope with the technical difficulty of measuring mass losses in thin film drying, an inverse method using Beck's sequential function specification was used. Superficial heat flux density was estimated from internal temperature measurements and masses losses computed from an energy balance. This method proved to be more accurate than a mass balance method. These curves can be used as an ideal reference for drum dryer design.

Nomenclature

a	Thermal diffusivity	$m^2.s^{-1}$	A, B, C, D	Quadrupole elements	-
dt	Time step	s	δq	Step of heat flux density	$W.m^{-2}$
e_i	Sensor position	m	e	Copper plate thickness	m
$E(t)$	Cumulated energy density	$J.m^{-2}$	E'	Overall energy density	$J.m^{-2}$
$f(t)$	Inverse transfer function	-	$F(s)$	Transfer function	-
l_v	Latent heat of vaporization	$J.kg^{-1}$	M	Dry matter load	$kgDB.m^{-2}$
q	Interfacial heat flux density	$W.m^{-2}$	$R(t)$	Thermal resistance	$K.W^{-1}.m^2$
s	Laplace variable	s^{-1}	t	Time	s

T_i, T	Computed temperature	*°C or K*	T_b	Boiling temperature	*°C or K*
W	Dry base water content	*kg/kgDB*	Y_i	Experimental temperature	*°C or K*

Greeks letters

δ	increment	-	φ	Heat flux density	$W.m^{-2}$
ϕ	Heat flux density (Laplace)	-	λ	Copper thermal conductivity	$W.m^{-1}.K^{-1}$
θ	Temperature (Laplace)	-	ρc	Volumic thermal capacity	$J.m^{-3}.K^{-1}$

Subscript

0	Initial value	*f*	Final value

References

1. J. Vasseur, M. Loncin, High heat transfer coefficient in thin-film drying: application to drum drying, *Engineering and Food*, 217-225 (1984).

2. C. Carrère-Gée, Etude du séchage indirect d'une fine couche de boue d'hydroxyde d'aluminium en ébullition – Application au cylindre sécheur, PhD Dissertation, Université P. Sabatier, Toulouse - France (1999).

3. A. Degiovanni, Conduction dans un "mur" multicouche avec sources : extension de la notion de quadripole, *Int. J. Heat Mass Transfer* **31,** 553-557 (1988).

4. J. C. Batsale, D. Maillet, A. Degiovanni, Extension de la méthode des quadripoles thermiques à l'aide de transformations intégrales: calcul de transfert transfert thermique au travers d'un défaut plan bidimensionnel, *Int. J. Heat Mass Transfer* **37**, 111-127 (1994).

5. H. Stehfest, Remarks on algorithm 368. Numerical inversion of Laplace transform, A.C.M 53 (10) 624 (1970).

6. J. F. Beck, B. Blackwell, C. St. Clair, *Inverse Heat Conduction, Ill-posed Problems*, Wiley-Interscience, New York (1985).

7. C. Carrère-Gée, D. Lecomte, O. Fudym, B. Ladevie, J. Vasseur, Determination of heat flux in thin-layer drying of sludges, Proceedings of the 11th International Drying Symposium (IDS'98), Halkidiki, Greece, August 19-22, Vol. A, 695-702 (1998).